Control of spin current by a magnetic YIG substrate in NiFe/Al nonlocal spin valves

Dejene, F. K.; Vlietstra, N.; Luc, D.; Waintal, X.; Ben Youssef, J.; van Wees, B. J.

Published in:
Physical Review. B: Condensed Matter and Materials Physics

DOI:
10.1103/PhysRevB.91.100404

PHYSICAL REVIEW B **91**, 100404(R) (2015)

Control of spin current by a magnetic YIG substrate in NiFe/Al nonlocal spin valves

F. K. Dejene,[1,*] N. Vlietstra,[1] D. Luc,[2] X. Waintal,[2] J. Ben Youssef,[3] and B. J. van Wees[1]
[1]*Physics of Nanodevices, Zernike Institute for Advanced Materials, University of Groningen, NL-9747 AG Groningen, The Netherlands*
[2]*CEA-INAC/UJF Grenoble 1, SPSMS UMR-E 9001, F-38054 Grenoble, France*
[3]*Laboratoire de Magnetisme de Bretagne CNRS, Université de Bretagne Occidentale, 6 Avenue Le Gorgeu, F-29285 Brest, France*

(Received 19 December 2014; revised manuscript received 11 February 2015; published 24 March 2015)

We study the effect of a magnetic insulator [yttrium iron garnet (YIG)] substrate on the spin-transport properties of $Ni_{80}Fe_{20}$/Al nonlocal spin valve (NLSV) devices. The NLSV signal on the YIG substrate is about two to three times lower than that on a nonmagnetic SiO_2 substrate, indicating that a significant fraction of the spin current is absorbed at the Al/YIG interface. By measuring the NLSV signal for varying injector-to-detector distances and using a three-dimensional spin-transport model that takes spin-current absorption at the Al/YIG interface into account, we obtain an effective spin-mixing conductance $G_{\uparrow\downarrow} \simeq 5\text{–}8 \times 10^{13}\ \Omega^{-1}\,\text{m}^{-2}$. We also observe a small, but clear, modulation of the NLSV signal when rotating the YIG magnetization direction with respect to the fixed spin polarization of the spin accumulation in the Al. Spin relaxation due to thermal magnons or roughness of the YIG surface may be responsible for the observed small modulation of the NLSV signal.

DOI: 10.1103/PhysRevB.91.100404 PACS number(s): 72.25.Ba, 72.25.Hg, 72.25.Mk, 75.47.Lx

The coupled transport of spin, charge, and heat in nonmagnetic (N) metals deposited on the magnetic insulator $Y_3Fe_5O_{12}$ (YIG) has led to new spin caloritronic device concepts, such as thermally driven spin currents, the generation of spin angular momentum via the spin Seebeck effect (SSE) [1], spin pumping from YIG to metals [2], spin-orbit coupling (SOC) induced magnetoresistance effects [3,4], and the spin Peltier effect, i.e., the inverse of the SSE that describes cooling or heating by spin currents [5]. In these spin caloritronic phenomena, the spin-mixing conductance $G_{\uparrow\downarrow}$ of the N/YIG interface controls the transfer of spins from the conduction electrons in N to the magnetic excitations (magnons) in the YIG, or vice versa [6–10]. The interconversion of a spin current to a voltage employs the (inverse) spin Hall effect in heavy metals such as Pt or Pd. The possible presence of proximity induced magnetism in these metals is reported to introduce spurious magnetothermoelectric effects [11,12] or enhance $G_{\uparrow\downarrow}$ [7]. Owing to the short spin-diffusion length λ in these large SOC metals, the applicability of the diffusive spin-transport model is also questionable. Experimental measurements that alleviate these concerns are, however, scarce and hence are highly required.

In this Rapid Communication, we investigate the interaction of a spin current (in the absence of a charge current) with the YIG magnetization employing the nonlocal spin valve (NLSV) geometry [13–15]. Using a metal with low SOC and long spin-diffusion length allows us to treat our experiment using the diffusive spin-transport model. We find that the NLSV signal on the YIG substrate is two to three times lower than that on the SiO_2 substrate, indicating significant spin-current absorption at the Al/YIG interface. By varying the angle between the induced spin accumulation and the YIG magnetization direction we observe a small, but clear, modulation of the NLSV signal. We also find that modifying the quality of the Al/YIG interface, using different thin-film deposition methods [4], influences $G_{\uparrow\downarrow}$ and hence the size of the spin current flowing at the Al/YIG interface. Recently, a low-temperature measurement of a similar effect was reported by Villamor *et al.* [16] in Co/Cu devices where $G_{\uparrow\downarrow} \sim 10^{11}\ \Omega^{-1}\,\text{m}^{-2}$ was estimated, two orders of magnitude lower than in the literature [4,8]. Here, we present a room-temperature spin-transport study in transparent $Ni_{80}Fe_{20}$ (Py)/Al NLSV devices.

Figure 1 depicts the concept of our experiment. A nonmagnetic metal (green) deposited on the YIG connects the two in-plane polarized ferromagnetic metals F_1 and F_2, which are used for injecting and detecting spin currents, respectively. A charge current through the F_1/Al interface induces a spin accumulation $\boldsymbol{\mu}_s(\vec{r}) = (0,\mu_s,0)^T$ that is polarized along the $\hat{y}$ direction, parallel to the magnetization direction of F_1. This nonequilibrium $\boldsymbol{\mu}_s$, the difference between the electrochemical potentials for spin up and spin down electrons, diffuses to both $+\hat{x}$ and $-\hat{x}$ directions of the F_1/Al interface with an exponential decay characterized by the spin-diffusion length λ_N. Spins arriving at the detecting F_2/Al interface give rise to a nonlocal voltage V_{nl} that is a function of the relative magnetic configuration of F_1 and F_2, being minimum (maximum) when F_1 and F_2 are parallel (antiparallel) to each other.

For NLSV devices on a SiO_2 substrate, spin relaxation proceeds via electron scattering with phonons, impurities, or defects present in the spin-transport channel, also known as the Elliot-Yafet (EY) mechanism. The situation is different for a NLSV on the magnetic YIG substrate where additional spin relaxation due to thermal magnons in the YIG and/or interfacial spin-orbit coupling can be mediated by direct spin-flip scattering or spin precession. Depending on the magnetization direction $\hat{m}$ of the YIG with respect to $\boldsymbol{\mu}_s$, spins incident at the Al/YIG surface are absorbed ($\hat{m} \perp \boldsymbol{\mu}_s$) or reflected ($\hat{m} \parallel \boldsymbol{\mu}_s$), thereby causing a spin-current density $\boldsymbol{j}_s$ through the Al/YIG interface [9],

$$\boldsymbol{j}_s(\hat{m})|_{z=0} = G_r \hat{m} \times (\hat{m} \times \boldsymbol{\mu}_s) + G_i(\hat{m} \times \boldsymbol{\mu}_s) + G_s \boldsymbol{\mu}_s. \quad (1)$$

Here $\hat{m} = (m_x,m_y,0)^T$ is a unit vector parallel to the in-plane magnetization of the YIG, G_r (G_i) is the real (imaginary)

*f.k.dejene@gmail.com

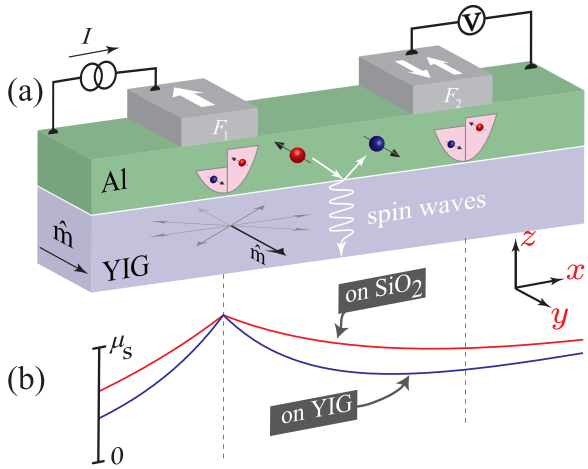

FIG. 1. (Color online) Concept of the experiment for $\hat{m} \parallel \boldsymbol{\mu}_s$. (a) A charge current through the F_1/Al interface creates a spin accumulation $\boldsymbol{\mu}_s$ in the Al. The diffusion of $\boldsymbol{\mu}_s$ to the F_2/Al interface is affected by spin-flip relaxation at the Al/YIG interface. Scattering of a spin up electron ($s = \hbar/2$) into a spin down electron ($s = -\hbar/2$) is accompanied by magnon emission ($s = \hbar$), creating a spin current into the YIG that is minimum (maximum) when $\hat{\mu}_s$ is parallel (perpendicular) to the magnetization of the YIG. (b) Profile of $\boldsymbol{\mu}_s$ along the Al strip on a SiO_2 (red) and YIG (blue) substrate. The spin accumulation at the F_2/Al is lower for the YIG substrate compared to that on SiO_2.

part of the spin-mixing conductance per unit area, and G_s is a spin-sink conductance that can be interpreted as an effective spin-mixing conductance that quantifies spin-absorption (flip) effects that is independent of the angle between $\hat{m}$ and $\boldsymbol{\mu}_s$.

When $\hat{m} \parallel \boldsymbol{\mu}_s$, some of the spins incident on the YIG are reflected back into the Al while some fraction is absorbed by the YIG. The absorption of the spin current in this collinear case is governed by a spin-sink effect either due to (i) the thermal excitation of the YIG magnetization (thermal magnons) or (ii) spin-flip processes due to interface spin-orbit effects or magnetic impurities present at the interface. This process can be characterized by an effective spin-mixing interface conductance G_s which, at room temperature, is about 20% of G_r [5]. Because of this additional spin-flip scattering, the maximum NLSV signal on the YIG substrate should also be smaller than that on the SiO_2. When $\hat{m} \perp \boldsymbol{\mu}_s$, spins arriving at the Al/YIG interface are absorbed. In this case all three terms in Eq. (1) contribute to a maximum flow of spin current through the interface. The nonlocal voltage measured at F_2 is hence a function of the angle between $\hat{m}$ and $\boldsymbol{\mu}_s$ and should reflect the symmetry of Eq. (1).

Figure 2(a) shows the scanning electron microscope image of the studied NLSV device that was prepared on a 200-nm-thick single-crystal YIG, having a very low coercive field [2,4,17], grown by liquid phase epitaxy on a 500-μm-thick (111) $Gd_3Ga_5O_{12}$ (GGG) substrate. It consists of two 20-nm-thick $Ni_{80}Fe_{20}$ (Py) wires connected by a 130-nm-thick Al cross. A 5-nm-thick Ti buffer layer was inserted underneath the Py to suppress direct exchange coupling between the Py and YIG. We studied two types of devices, hereafter referred to as type-A and type-B devices. In type-A devices (four devices), prior to the deposition of the Al (by electron-beam evaporation), Ar ion milling of the Py surface was performed to ensure a transparent Py/Al interface. This process, however, introduces unavoidable milling of the YIG surface, thereby introducing a disordered Al/YIG interface with lower $G_{\uparrow\downarrow}$ [18]. To circumvent this problem, in type-B devices (two devices), we first deposit a 20-nm-thick Al strip (by dc sputtering) between the injector and detector Py wires. Sputtering is reported to yield a better interface [4]. Next, after Ar ion milling of the Py and sputtered-Al surfaces, a 130-nm-thick Al layer was deposited using electron-beam evaporation. Similar devices prepared on a SiO_2 substrate were also investigated. All measurements were performed at room temperature using standard low-frequency lock-in measurements.

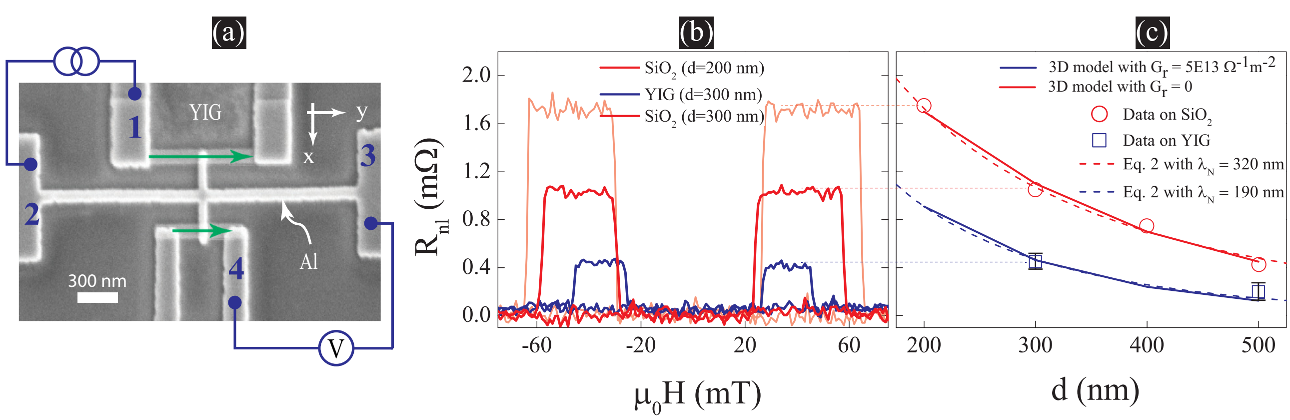

FIG. 2. (Color online) (a) Scanning electron microscope image of the measured type-A device. Two Py wires (indicated by green arrows) are connected by an Al cross. A charge current I from contact 1 to 2 creates a spin accumulation at the F_1/Al interface that is detected as a nonlocal spin voltage V_{nl} using contacts 3 and 4. (b) The NLSV resistance $R_{nl} = V_{nl}/I$ for representative YIG (blue) and SiO_2 (red and orange) NLSV samples. For comparison, a constant background resistance has been subtracted from each measurement. (c) Dependence of the NLSV signal on the spacing d between the injecting and detecting ferromagnetic wires together with calculated spin signal values using a 1D (dashed lines) and 3D (solid lines) spin-transport model. For each distance d between the injector and detector, several devices were measured, with the error bars indicating the spread in the measured signal.

The NLSV resistance $R_{\rm nl} = V_{\rm nl}/I$ as a function of the applied in-plane magnetic field (along $\hat{y}$) is shown in Fig. 2(b), both for SiO_2 (red and orange) and YIG (blue) samples. Note that the magnetizations of the injector, detector, and YIG are all collinear and hence no initial transverse spin component is present. The spin valve signal, defined as the difference between the parallel R_P and antiparallel R_{AP} resistance values $R_{\rm SV} = R_P - R_{AP}$ on the YIG substrate, is about two to three times smaller than that on the SiO_2 substrate. This reduction in the NLSV signal indicates the presence of an additional spin-relaxation process even for $\hat{m} \parallel \boldsymbol{\mu}_s$. Assuming an identical spin injection efficiency in both devices, this means that spin relaxation in the Al on the YIG substrate occurs on an effectively shorter spin-relaxation length λ_N. To properly extract λ_N we performed several measurements for varying distances between the Py wires, as shown in Fig. 2(c) both on SiO_2 (red circle) and YIG (blue square) substrates. Also shown are dashed-line fits using the expression for the nonlocal spin valve signal $R_{\rm SV}$ obtained from a one-dimensional spin-transport theory given by [14]

$$R_{\rm SV} = \frac{\alpha_F^2 R_N e^{-d/2\lambda_N}}{\left(\frac{R_F}{R_N}+1\right)\left[\frac{R_F}{R_N}\sinh(d/2\lambda_N)+\cosh(d/2\lambda_N)\right]}. \quad (2)$$

Here $R_F = (1-\alpha_F^2)\frac{\lambda_F}{\sigma_F}$ and $R_N = \frac{\lambda_N}{\sigma_N}$ are spin area resistances of the ferromagnetic (F) and nonmagnetic (N) metals, respectively. λ_N and λ_F are the corresponding spin-diffusion lengths, σ_F (σ_N) is the electrical conductivity of the F (N), α_F is the spin polarization of F, and d is the distance between the injecting and detecting ferromagnetic electrodes. Fitting the SiO_2 data using Eq. (2), we extract $\alpha_F = 0.32$ and $\lambda_{N,\rm SiO_2} = 320$ nm, which are both in good agreement with reported values [13–15]. A similar fitting procedure for the YIG data, assuming an identical spin injection efficiency, yields an effectively shorter spin-diffusion length $\lambda_{N,\rm YIG} =$ 190 nm due to the additional spin-flip scattering at the Al/YIG interface. This value of $\lambda_{N,\rm YIG}$ therefore contains important information regarding an effective spin-mixing conductance G_s that can be attributed to the interaction of spins with thermal magnons in the YIG. When spin precession, due to the applied external field as well as the effective field due to G_i, is disregarded, we can now estimate G_s by relating $\lambda_{N,\rm YIG}$ to $\lambda_{N,\rm SiO_2}$ via G_s as (see the Supplemental Material [19], Sec. I)

$$\frac{1}{\lambda_{N,\rm YIG}^2} = \frac{1}{\lambda_{N,\rm SiO_2}^2} + \frac{1}{\lambda_r^2}, \quad (3)$$

with $\lambda_r^{-2} = 2G_s/t_{\rm Al}\sigma_N$ [19]. Using the extracted values from the fit, $\sigma_N = 2\times10^7$ S/m and $t_{\rm Al} = 130$ nm, we extract $G_s \simeq 2.5\times10^{13}\ \Omega^{-1}\,{\rm m}^{-2}$, which is about 25% of the maximum $G_r \sim 10^{14}\ \Omega^{-1}\,{\rm m}^{-2}$ reported for Pt/YIG [4,7] and Au/YIG [8] interfaces.

To quantify our results we performed three-dimensional finite element simulations using COMSOL MULTIPHYSICS (3D-FEM) [19,20] that uses a set of equations that is equivalent to the continuous random matrix theory in three dimensions (CRMT3D) [21]. The charge current $j_c^\alpha(\vec{r})$ and spin current $\boldsymbol{j}_s^\alpha(\vec{r})$ (where $\alpha \in x,y,z$) are linked to their corresponding driving forces via the electrical conductivity as

$$\begin{pmatrix} j_c^\alpha(\vec{r}) \\ \boldsymbol{j}_s^\alpha(\vec{r}) \end{pmatrix} = -\begin{pmatrix} \sigma & \alpha_F\sigma \\ \alpha_F\sigma & \sigma \end{pmatrix}\begin{pmatrix} \vec{\nabla}\mu_c \\ \vec{\nabla}\boldsymbol{\mu}_s \end{pmatrix}, \quad (4)$$

where $\mu_c = (\mu_\uparrow + \mu_\downarrow)/2$ and $\boldsymbol{\mu}_s = (\mu_\uparrow - \mu_\downarrow)/2$ are the charge and spin accumulation chemical potentials, respectively. We supplement Eq. (4) by the conservation laws for charge current, $\nabla\cdot j_c^\alpha(\vec{r}) = 0$, and spin current, $\nabla\cdot\boldsymbol{j}_s = (1-\alpha_F^2)\sigma[\boldsymbol{\mu}_s/\lambda^2 + \vec{\omega}_L\times\boldsymbol{\mu}_s]$, where $\vec{\omega}_L = g\mu_B\vec{B}/\hbar$, with $g = 2$ is the Larmor precession frequency due to spin precession in an in-plane magnetic field $\vec{B} = (B_x,B_y,0)^T$ and μ_B is the Bohr magneton (see the Supplemental Material [19], Sec. II). To include spin mixing at the Al/YIG interface we impose continuity of the spin current $\boldsymbol{j}_s$ at the interface using Eq. (1). The input material parameters such as σ, λ, and α_F are taken from Refs. [22,23].

The calculated spin signals obtained from our 3D-FEM are shown in Fig. 2(c) for samples on SiO_2 (red solid line) and YIG (blue solid line) substrates. By matching the

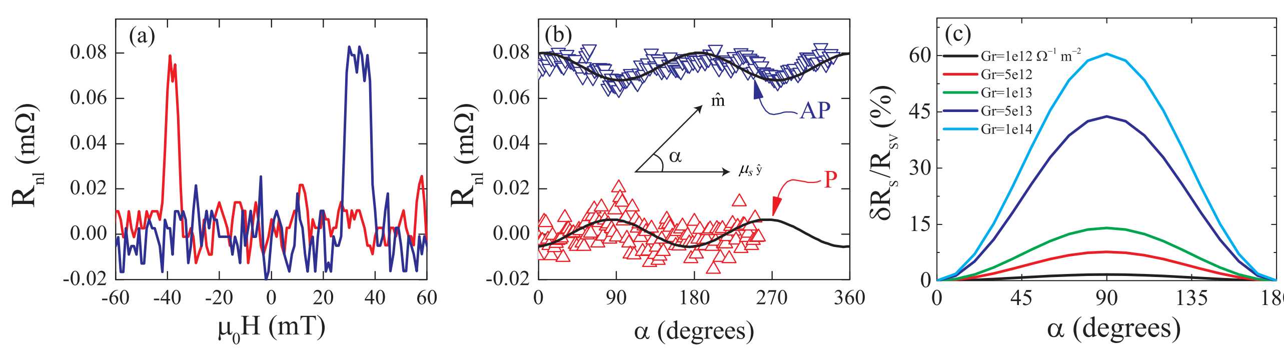

FIG. 3. (Color online) (a) Nonlocal spin valve resistance $R_{\rm nl}$ of a type-B device with $d = 500$ nm between injecting and detecting Py wires and $t_{\rm Al} = 130$ nm. A constant background resistance of 117 mΩ was subtracted from the original data. (b) Angular dependence of the NLSV signal in the parallel and antiparallel configurations. The AP curve is an average of ten measurements and that of the P state is a single scan. Both resistance states exhibit a $\cos(2\alpha)$ dependence on the angle between $\hat{m}$ and $\boldsymbol{\mu}_s$. The black solid lines are calculated using the 3D-FEM model for $G_r = 1\times10^{13}\ \Omega^{-1}\,{\rm m}^{-2}$ that show a percentage modulation of only 12% corresponding to the green curve in (c) $\delta R_{\rm SV}/R_{\rm SV}$. The angular dependent measurement in (b) is from a device for which a complete set of measurements was performed. A spin valve measurement as in (a) was also performed for another device with $d = 300$ nm.

experimentally measured NLSV signal on the SiO_2 substrate with the calculated values in the model we obtain $\alpha_F = 0.3$ and $\lambda_N = 350$ nm. Using these two values and setting $G_s \simeq 5 \times 10^{13}\ \Omega^{-1}\,\mathrm{m}^{-2}$ well reproduces the measured spin signal on the YIG substrate. This obtained value of G_s obtained here is consistent with that extracted from our one-dimensional (1D) analysis based on Eq. (2). Hence, the interaction of spins with the YIG magnetization, as modeled here, can capture the concept of spin-mixing conductance being responsible for the observed reduction in the spin signal.

In the following we investigate the dependence of R_{nl} on the angle α between $\boldsymbol{\mu}_s$ and $\hat{m}$. We rotate the sample under the application of a very low in-plane magnetic field $B \leqslant 5$ mT, enough to saturate the low-coercive ($\leqslant 0.5$ mT) YIG magnetization [4,5] but smaller than the coercive fields of F_1 and F_2 ($\sim$20 mT). This condition is important to maintain fixed polarization axes of $\boldsymbol{\mu}_s$, along the magnetization direction of the injecting ferromagnet, and also have a well defined α. The result of such measurement in a type-B device is shown in Fig. 3(b) for $d = 400$ nm between F_1 and F_2. Although the measured NLSV signal [Fig. 3(a)] is smaller than in type-A devices, possibly due to a better Al/YIG interface, R_{nl} exhibits a $\cos(2\alpha)$ behavior with a maximum (minimum) for $\alpha = 0$ ($\alpha = \pi/2$), consistent with Eq. (1). However, the maximum change (modulation) of the signal $\delta R_s = R_{\mathrm{nl}}(\alpha = 0) - R_{\mathrm{nl}}(\alpha = \pi/2)$ is only 12% of the total spin signal R_{SV}, which is at odds with the large spin-mixing conductance estimated from Fig. 2(b). From anistropic magnetoresistance measurements we exclude the possibility of any rotation of the magnetization of the injector and detector as the cause for the observed modulation in the NLSV signal (see the Supplemental Material [19], Sec. III B).

Using the 3D-FEM we calculated the angular dependence of R_{SV} for various values of G_r, where the percentage modulation $\delta R_s/R_{\mathrm{SV}}$ is plotted as a function of α, as shown in Fig. 3(c). The G_r value of $1 \times 10^{13}\ \Omega^{-1}\,\mathrm{m}^{-2}$ extracted from the NLSV signal modulation experiment is one order of magnitude less than reported for Pt [4]. This can be possibly caused by the presence of a disordered Al/YIG interface with an rms roughness of 0.8 nm [as measured by atomic force microscopy (AFM)], which is close to the magnetic coherence volume $\sqrt[3]{V_c} \simeq 1.3$ nm [6] of the YIG. This length scale determines the effective width of the Al/YIG interface and also the extent to which spin current from the Al is felt by the YIG magnetization [6,24]. Furthermore, the fact that there exists a finite spin mixing when $\alpha = 0$, as discussed above, can also explain why the observed modulation is small. It is important to note that in our experiments the nonequilibrium spin accumulation induced by electrical spin injection into Al has a spin polarization strictly along the direction of the magnetization of F_1, which lies along the $\hat{y}$ axis. In the measurement results shown in Figs. 1(b) and 2(b) the magnetization of the F_2 is always kept either parallel or antiparallel to the detector F_1. This ensures that it is only the $\hat{y}$ component of the spin accumulation that is measured in our experiments as it is insensitive to the other two spin-polarization directions. It is, however, possible that the interaction of the initially injected spin accumulation with the YIG magnetization, via $G_{\uparrow\downarrow}$, induces a finite NLSV signal with components polarized along the $\hat{x}$ and $\hat{z}$ directions.

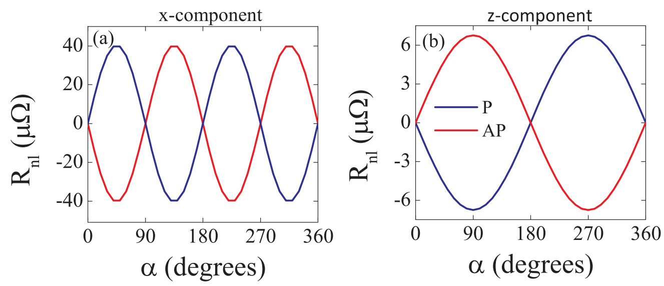

FIG. 4. (Color online) Calculated NLSV signals showing the (a) $\hat{x}$ component and (b) $\hat{z}$ component of the NLSV signal R_{nl} in the parallel (red) and antiparallel (blue) magnetization configurations of the injector and detector ferromagnetic contacts for $G_r = 1 \times 10^{13}\ \Omega^{-1}\,\mathrm{m}^{-2}$ and $G_i = 0.1 G_r$. Even if the injected spin accumulation is polarized along the magnetization direction of the injecting electrode F_1, its interaction with the magnons via the spin-mixing conductance induces these spin accumulation components.

Figure 4 shows the angular dependence of the $\hat{x}$ and $\hat{z}$ component of the NLSV signal as calculated using our 3D-FEM. While the $\hat{z}$ component exhibits a $\sin(\alpha)$ dependence, the $\hat{x}$ component shows a $\sin(2\alpha)$ dependence which is consistent with Eq. (1). The size of the modulation is determined by G_r for the $\hat{x}$ component and by G_i for the $\hat{z}$ component. In a collinear measurement configuration these transverse spin accumulation components can induce local magnetization dynamics by exerting a spin transfer torque to the YIG. Separately measuring these spin accumulations using ferromagnetic contacts magnetized along the $\hat{x}$ and $\hat{z}$ directions can be an alternative way to extract $G_{\uparrow\downarrow}$.

In summary, we studied spin injection and relaxation at the Al/YIG interface in $Ni_{80}Fe_{20}$/Al lateral spin valves fabricated on YIG. The samples on the YIG substrate yield NLSV signals that are two to three times lower than those grown on standard SiO_2 substrates, indicating spin-current absorption by the magnetic YIG substrate. We also observed a small, but clear, modulation of the measured NLSV signal as a function of the angle between the spin accumulation and magnetization of the YIG. The presence of a disordered Al/YIG interface combined with a spin-flip (sink) process due to thermal magnons or interface spin-orbit effects can be accounted for this small modulation. Using finite element magnetoelectronic circuit theory as well as additional control experiments, we establish the concept of collinear (effective) spin-mixing conductance due to the thermal magnons in the YIG. Our result therefore calls for the inclusion of this term in the analysis of spintronic and spin caloritronic phenomena observed in metal/YIG bilayer systems.

The authors thank M. de Roosz and J. G. Holstein for technical assistance. This work is part of the research program of the Foundation for Fundamental Research on Matter (FOM) and is supported by NanoLab NL, NanoNextNL, a micro- and nanotechnology consortium of the Government of the Netherlands and 130 partners, InSpin EU-FP7-ICT Grant No. 612759, and the Zernike Institute for Advanced Materials.

[1] K. Uchida, J. Xiao, H. Adachi, J. Ohe, S. Takahashi, J. Ieda, T. Ota, Y. Kajiwara, H. Umezawa, H. Kawai *et al.*, Nat. Mater. **9**, 894 (2010).

[2] V. Castel, N. Vlietstra, J. Ben Youssef, and B. J. van Wees, Appl. Phys. Lett. **101**, 132414 (2012).

[3] M. Althammer, S. Meyer, H. Nakayama, M. Schreier, S. Altmannshofer, M. Weiler, H. Huebl, S. Geprägs, M. Opel, R. Gross, D. Meier, C. Klewe, T. Kuschel, J.-M. Schmalhorst, G. Reiss, L. Shen, A. Gupta, Y.-T. Chen, G. E. W. Bauer, E. Saitoh, and S. T. B. Goennenwein, Phys. Rev. B **87**, 224401 (2013).

[4] N. Vlietstra, J. Shan, V. Castel, B. J. van Wees, and J. Ben Youssef, Phys. Rev. B **87**, 184421 (2013).

[5] J. Flipse, F. K. Dejene, D. Wagenaar, G. E. W. Bauer, J. B. Youssef, and B. J. van Wees, Phys. Rev. Lett. **113**, 027601 (2014).

[6] J. Xiao, G. E. W. Bauer, K.-c. Uchida, E. Saitoh, and S. Maekawa, Phys. Rev. B **81**, 214418 (2010).

[7] X. Jia, K. Liu, K. Xia, and G. E. W. Bauer, Europhys. Lett. **96**, 17005 (2011).

[8] B. Heinrich, C. Burrowes, E. Montoya, B. Kardasz, E. Girt, Y.-Y. Song, Y. Sun, and M. Wu, Phys. Rev. Lett. **107**, 066604 (2011).

[9] Y.-T. Chen, S. Takahashi, H. Nakayama, M. Althammer, S. T. B. Goennenwein, E. Saitoh, and G. E. W. Bauer, Phys. Rev. B **87**, 144411 (2013).

[10] M. Weiler, M. Althammer, M. Schreier, J. Lotze, M. Pernpeintner, S. Meyer, H. Huebl, R. Gross, A. Kamra, J. Xiao, Y.-T. Chen, H. J. Jiao, G. E. W. Bauer, and S. T. B. Goennenwein, Phys. Rev. Lett. **111**, 176601 (2013).

[11] S. Y. Huang, X. Fan, D. Qu, Y. P. Chen, W. G. Wang, J. Wu, T. Y. Chen, J. Q. Xiao, and C. L. Chien, Phys. Rev. Lett. **109**, 107204 (2012).

[12] T. Kikkawa, K. Uchida, S. Daimon, Y. Shiomi, H. Adachi, Z. Qiu, D. Hou, X.-F. Jin, S. Maekawa, and E. Saitoh, Phys. Rev. B **88**, 214403 (2013).

[13] F. J. Jedema, A. T. Filip, and B. J. van Wees, Nature (London) **410**, 345 (2001).

[14] F. J. Jedema, M. S. Nijboer, A. T. Filip, and B. J. van Wees, Phys. Rev. B **67**, 085319 (2003).

[15] T. Kimura, T. Sato, and Y. Otani, Phys. Rev. Lett. **100**, 066602 (2008).

[16] E. Villamor, M. Isasa, S. Vélez, A. Bedoya-Pinto, P. Vavassori, L. E. Hueso, F. S. Bergeret, and F. Casanova, Phys. Rev. B **91**, 020403 (2015).

[17] V. Castel, N. Vlietstra, B. J. van Wees, and J. B. Youssef, Phys. Rev. B **86**, 134419 (2012).

[18] Z. Qiu, K. Ando, K. Uchida, Y. Kajiwara, R. Takahashi, H. Nakayama, T. An, Y. Fujikawa, and E. Saitoh, Appl. Phys. Lett. **103**, 092404 (2013).

[19] See Supplemental Material at http://link.aps.org/supplemental/10.1103/PhysRevB.91.100404 for the derivation of Eq. (3), a detailed description of the finite element model, and additional data to the main article.

[20] A. Slachter, F. L. Bakker, and B. J. van Wees, Phys. Rev. B **84**, 174408 (2011).

[21] V. S. Rychkov, S. Borlenghi, H. Jaffres, A. Fert, and X. Waintal, Phys. Rev. Lett. **103**, 066602 (2009).

[22] F. L. Bakker, A. Slachter, J.-P. Adam, and B. J. van Wees, Phys. Rev. Lett. **105**, 136601 (2010).

[23] F. K. Dejene, J. Flipse, G. E. W. Bauer, and B. J. van Wees, Nat. Phys. **9**, 636 (2013).

[24] M. Schreier, A. Kamra, M. Weiler, J. Xiao, G. E. W. Bauer, R. Gross, and S. T. B. Goennenwein, Phys. Rev. B **88**, 094410 (2013).